Frequency Selective Surface with Miniaturized Elements: a Different Approach

Muaad Hussein, Yi Huang and Jiafeng Zhou (jiafeng.zhou@liverpool.ac.uk)

University of Liverpool, UK

Abstract: Recently, many approaches have been proposed to miniaturize the dimensions of frequency selective surface (FSS) array elements. This is usually achieved by increasing the equivalent electrical lengths of array elements. In this paper, a different approach is proposed to realize the miniaturization by making use of the capacitance between adjacent layers of an FSS. Such an FSS will not only have a very small element size, but also have an extremely low profile. The element size is one of the smallest reported so far to the authors' best knowledge.

1 Introduction

A frequency selective surface (FSS) is formed by periodic arrays of usually metallic elements on a dielectric substrate. The geometry of the surface in one period (array element) determines the frequency response of an FSS. Various responses can be achieved by using different traditional FSS element shapes. An FSS often displays selectivity not only on the frequency, but also on the angle and polarization of the incident wave. FSS can be constructed by using identical elements arranged in a one- or two-dimension infinite array.

Fig. 1. FSS in different military and civil applications [18]**.**

The equivalent circuit for a bandstop FSS or a bandpass FSS is the combination of *LC* in series or in parallel, respectively [1] [2]. Many different shapes have been used to construct an FSS. The equivalent FSS circuit is directly related to the array element size, shape and the polarization. Equivalent circuits and analysis of some of the traditional structures can be found in [2][3].

FSSs have been most commonly used in microwave and optical frequency regions of the electromagnetic spectrum and for applications such as antennas, radomes, radio frequency absorbers, wireless securities to electromagnetic (EM) shielding applications and metamaterials [2] [4][5][6][7][8][9]. Decreasing loss in antennas and improving the radiated power are successfully realized by using these structures [10][11]. They are designed to reflect, transmit or absorb electromagnetic radiation at different frequencies [1][12][13]. The use of dual-reflector antennas in space missions such as Galileo, Cassini, Cassegrain and Voyager, sharing the main reflector among different frequency bands, has been made possible by using an FSS [14][15][16][17].

FSSs are widely used in modern military platforms such as aircraft, ships and missiles, as can be seen from Fig. 1

[18]. FSSs can be used in many applications in the civil sector as well, such as the isolation of unwanted and harmful radiation in L-band and S-band in hospitals, schools and domestic environments [19][20][21].

2 Motivations

FSSs with miniaturized elements can achieve stable performance against the incident angle of illuminating waves. The plane of incidence and polarization of incidence are defined in Fig. 2. For normal incidence, the FSS is excited by an electromagnetic wave with the propagation vector (**k**) towards the *z* axis, a magnetic field vector (**H**) towards the *x* axis and an electric field vector (**E**) towards the *y* axis direction. For other incidence, ɵ represents the incident angle, while ϕ is the polarization angle.

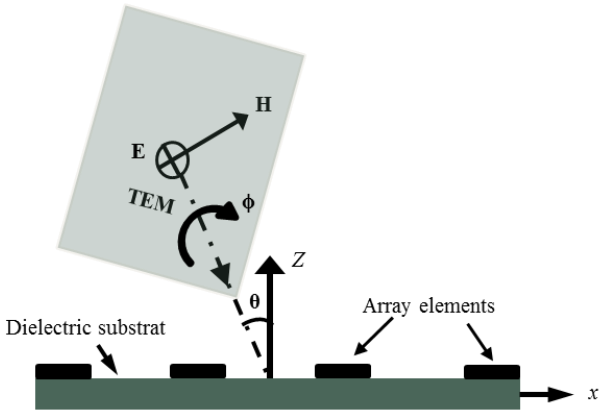

Fig. 2. The plane of incident wave, ɵ is the angle of incidence, ϕ is the polarisation angle.

Recently, many approaches have been proposed to miniaturize FSS array element dimensions. For example, a parallel lumped inductor and a lumped capacitor can be used to reduce the size of the FSS array element [22][23]. Adding meander-slots to the circular ring structure can produce FSSs with array element dimensions much smaller than the wavelength [24]. A study in [25] demonstrated a miniature FSS by printing micro wire on a dielectric. Printing four symmetrical spiral patterns of metallic meander lines can increase the electrical length of the array element and increase the value of the resonant components [26]. However, increasing the electrical length of an array element with the same physical dimensions has limitations, and could increase the complexity of the FSS structure. Thus, a parallel lumped inductor and lumped capacitor can be used to design a dually polarized FSS array element in [22]. Two metallic layers of an asymmetrical pattern are placed on the top and bottom side of a dielectric substrate to achieve a dually polarized frequency response in [27].

Traditionally, the element of a FSS is rotationally symmetrical and the element arrays in a multi-layer FSS are aligned with each other. Different techniques have been used to achieve stable frequency responses in different polarizations for single and multi-layer FSSs under various angles of incident waves. Accomplishing a symmetrical FSS array element can contribute to achieving a stable resonance with respect to the polarization and the angle of incidence [22][23][24][25][26][28]. However, using symmetrical array element shapes to avoid polarization sensitivity can restrict FSS design options.

3. The Proposed FSS Element

In this paper, a novel approach to design a miniaturized FSS is proposed. The array element is realized by using stepped-impedance transmission lines. This is done by using a wire to control the path of the current which passes through the metallic surface of the element. Patches are added at the ends of the wire to enhance capacitance. As a result, the dimensions of the miniaturized element are much smaller than the wavelength at the resonant frequency. The periodicity is 0.09λ.

Fig. 3 shows three cases of array element configuration. Fig. 3(a) shows the structure with a slot parallel to the *x* axis, while Fig. 3(b) illustrates the structure with a slot parallel to the *y* axis. The wire has an inductive effect and the slot has a capacitive effect. However, these two structures (Fig. 3(a) and (b)) are single polarized structures. A modification of the structure in Fig. 3(b) by adding a slot and micro-wires parallel to the *x* axis is shown in Fig. 3(c). This makes the structure dual polarized.

The equivalent circuit is a parallel *LC* circuit as shown in Fig. 4. The frequency response of the resonant element can be determined by evaluating the capacitance and inductance of the array element. The value of the inductance *L* is determined by:

$$L = \mu_o \mu_e \frac{P}{2n\pi}[\ln \operatorname{cosec}(\frac{\pi w}{2P})] \tag{4.1}$$

where L is the strip inductance, which is determined by the strip length P, the strip width w and the effective magnetic permeability μ_e of the structure. n is the number of metal layers. The value of the capacitance C is determined by

$$C = n\varepsilon_o \varepsilon_e \frac{2b}{\pi}[\ln \operatorname{cosec}(\frac{\pi g}{2b})] \tag{4.2}$$

where C is the intrinsic capacitance between the two adjacent patches in each layer, which is determined by the patch length b, the gap g between adjacent patches and the effective dielectric constant ε_e of the structure, $\varepsilon_e \approx (\varepsilon_r+1)/2$.

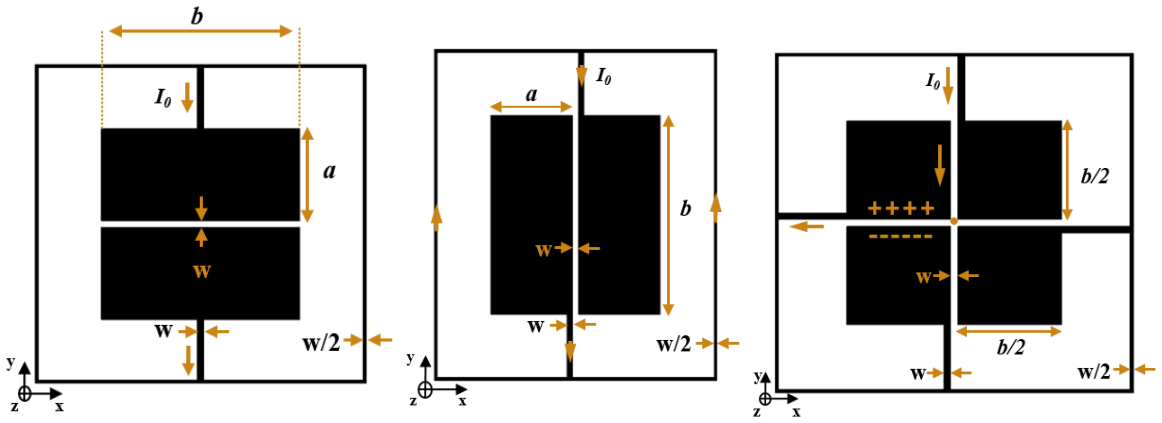

(a) **(b)** **(c)**

Fig. 3. Array element of the proposed FSS structures, (a) the single polarized element with the slot towards the x-axis, (b) the single polarized element with the slot towards the y-axis and (c) the dual polarized array element.

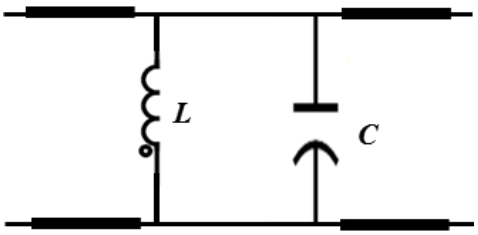

Fig. 4. The equivalent circuit of the proposed FSS structure.

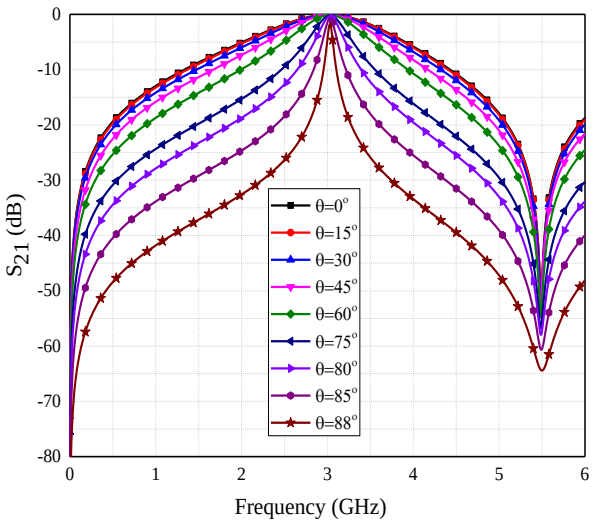

Fig. 5. The transmission coefficient of the proposed FSS as a function of the incident angle.

The resonator was designed on a 1.5 mm thick FR4 substrate with a relative dielectric constant of ε_r=4.3. The length of the square patch b is 6 mm. The slot width and wire width are 0.2 mm. The periodic constant P of the array is 9 mm.

The resonant frequency of the proposed structure as shown Fig. 3(c) is insensitive to the angle of incidence (θ). The resonant frequency is stable with an incident angle up to 88°, although the bandwidth is decreased, as shown in Fig. 5.

A comparison of the FSS array element between the proposed structure and other reported miniaturized FSS elements is illustrated in Table I. It can be observed that the stepped-impedance FSS resonator is the smallest compared with other work.

Table I: Comparison of the element size with other references

FSS structure	Substrate Thickness (mm)	ε_r	Element size
[29]	1.6	4.3	0.22λ
[30]	1.6	4.3	0.104λ
[31]	0.5	3.55	0.088λ
[32]	0.127	2.2	0.067λ
[33]	1.6	5	0.061λ
The proposed dual polarized FSS	1.6	4.3	0.09λ
The proposed single polarized FSS	1.6	4.3	0.055λ

4 Multi-layer FSS Using the Proposed Elements

Fig. 6 shows the structure of the proposed single polarized FSS element, consisting of two metallic layers separated by a substrate layer. Each metallic layer is printed on one side of the dielectric substrate consisting of an inductive loop with a width of w and two capacitive patches, each with an area of $b \times a$. Numerical analysis of the proposed element was performed by using CST Microwave Studio, using unit cell boundary conditions to provide periodicity along the x and y axes.

The unique approached of the design is that ***the top and bottom layers are the same, but flipped in the xy plane***. In this way, the currents enter and exit from the top layer patches in opposite directions to the bottom layer patches, as shown in Fig. 7. This causes the charges to be distributed in different polarizations between the top and the bottom layers of the FSS, which induces a strong cross-layer capacitance, C_{cc}.

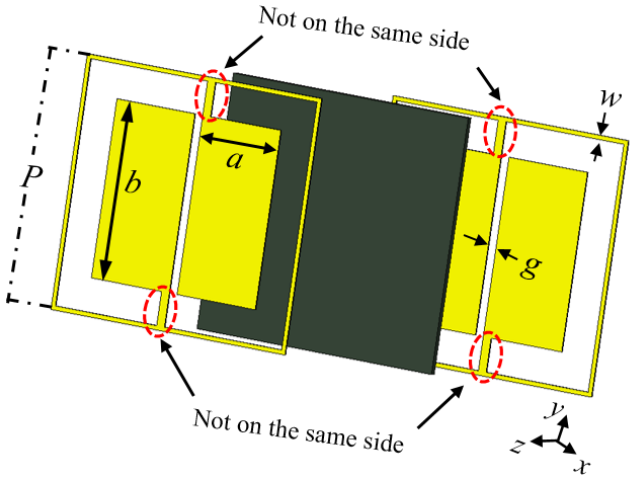

Fig. 6. Array element geometry of the proposed single polarized FSS.

For instance, when an external electrical field, **E**, is applied in the y-axis direction, the current will flow into the left patch and out from the right patch towards the ($-y$) axis direction on the top layer, as shown in Fig. 7(a). This can induce positive charges on the left patch of the proposed element and negative charges on the right one. On the other hand, in

the bottom layer, since the structure is flipped, the current will flow into the right patch and out from the left patch towards the (-*y*) axis direction, as shown in Fig. 7(b). This can induce charges opposite to the top layer. Thus, there is a strong cross-layer capacitance existing between the top and the bottom layer.

This capacitance offers significant advantages to the FSS element by making the structure compact, low-profile (the lower the profile, the stronger the capacitance) and insensitive to surrounding dielectric materials, as discussed in the following sections.

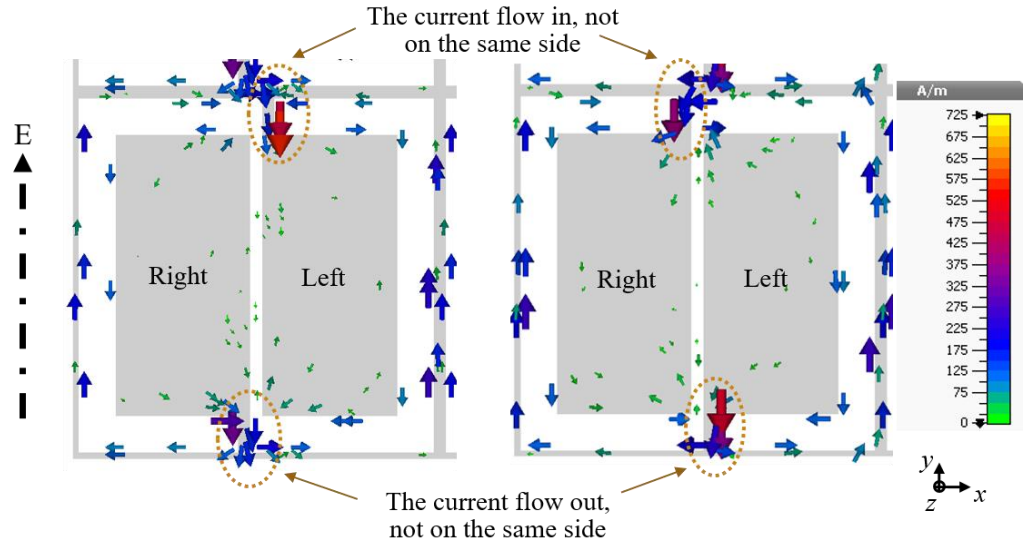

(a) **(b)**

Fig. 7. Current distribution of the proposed element on (a) the top layer, and (b) the bottom layer.

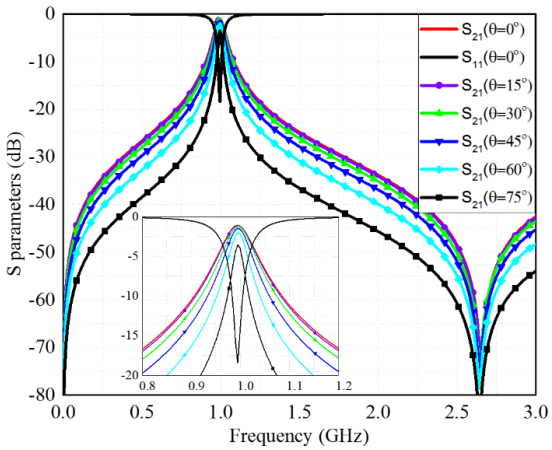

Fig. 8. Simulated frequency response of the proposed two-layer FSS under variable incident angles for the vertical polarisation.

The proposed structure is designed on an FR4 substrate. The two metallic layers are etched on the top and bottom copper layers of a 0.127 mm-thick FR4 substrate with a dielectric constant of 4.3 and a loss tangent of 0.025. The length of the rectangle patch (*b*) is 4.6 mm and the width (*a*) is 4.6 mm, the gap width g is 0.2 mm and the width, w, of the short line connecting the patches is 0.2 and for the loop is 0.1 mm. The periodic constant P of the array is 6 mm. Fig. 8 shows the simulated transmission and reflection coefficients. It can be seen that the resonant frequency is very stable against the incident angle up to 75˚.

The resonant frequency is 1 GHz with a fractional bandwidth of 6.1%. The reflection coefficient is -19 dB and the insertion loss is 1.13 dB at the resonant frequency. The size of the array element is found to be $0.02\lambda \times 0.02\lambda$**.**

The equivalent circuit model of the proposed array element for vertical polarized incident waves is shown in Fig. 9. It should be noted that the circuit model is only used to give a better qualitative understanding of the proposed structure. The actual equivalent circuit is much more complicated than this circuit model. The circuit model consists of an L_1C_1

circuit for the top layer structure, an L_2C_2 for the bottom layer structure and a cross-layer capacitor C_{cc} between them. The substrate between the two metallic layers acts as a transmission line of length h (h is the substrate thickness) and a characteristic impedance of Z. The transmission line is used here as a short circuit because h is very small. For example, at the resonant frequency 1 GHz, h is $\lambda/2362$ or 0.127 mm. In the circuit model, L_1 is equal to L_2 and C_1 is equal to C_2 due to symmetry.

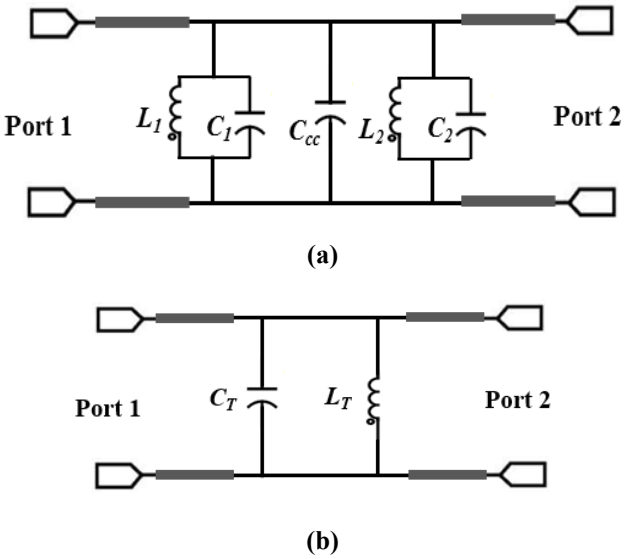

Fig. 9. Equivalent circuit of a two-metallic-layer structure, where $L_{T=}$ $(L_1+ L_2) / (L_1\times L_2)$ and $C_{r1}= C_1 + C_2 + C_{cc}$.

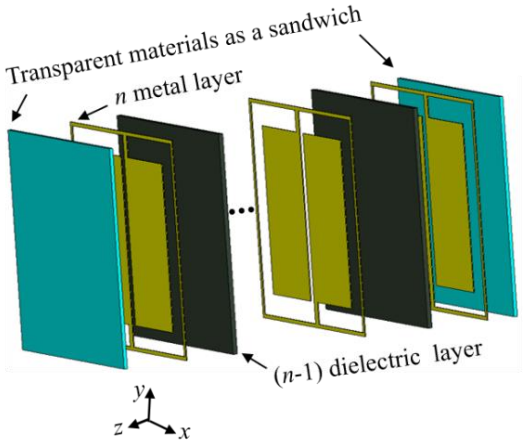

Fig. 10. Array element of the proposed n-metallic-layers FSS with thin dielectric supporters.

The cross-layer capacitance C_{cc} can be calculated by using the parallel plates' capacitance equation:

$$C_{cc} = (n-1)\frac{\varepsilon_r \varepsilon_o \mathrm{A}}{d} \tag{4.3}$$

The fringing effect can be ignored in this case because the gap between the two plates is very some small compared of with the size of the plates. The overlapping area of the conducting patch is A and equal to $2(a\times b)$; the parallel conducting layers are separated by a distance d, which is the thickness of the substrate h in this case, and the dielectric constant of the substrate is ε_r. It is quite obvious that the cross-layer capacitance is much higher than the intrinsic capacitance of each layer. The approximate theoretical values for the resonator components are $L_1 = L_2 = 3.5$ nH, $C_1 = C_2 = 0.28$ pF, while the value of $C_{cc} = 6.2$ pF. The value of C_{cc} is much greater as expected. The cross-coupling capacitance C_{cc} will significantly lower the resonant frequency of the FSS array element, which makes the element much more compact.

The cross-layer capacitance is higher with a thinner substrate (lower profile). This is contrary to the intrinsic capacitance. The intrinsic capacitance depends on the effective permittivity of the substrate. The effective permittivity is a function of the thickness of the substrate. If the thickness is comparable with the gap width, the effective permittivity is lower with a thinner substrate. The intrinsic capacitance is lower accordingly. If the substrate thickness is much

greater than the gap width, the effective permittivity is almost constant. Therefore, the proposed FSS with a lower profile is actually more compact, which is different from traditional structures.

Fig. 10 shows the structure with n metallic layers and (n-1) dielectric layers. The two transparent layers are only used to mechanically support assembling the multiple layers together if needed. There are alternative ways of doing this. For example, the layers can be thermally compressed together using a bonding film with a very thin thickness [34].

The simulated resonant frequency f, fractional bandwidth BW, lowest values of reflection coefficients S_{11} of a multi-layer FSS using the proposed design are summarized in Table II. The periodic dimension P is 6 mm, the same for all of these multi-layer structures. It shows that the increase of the number of layers n shifts the resonant frequency downward. For example, for n = 3 with two FR4 dielectric layers with a thickness of 0.127 mm for each, the resonant frequency is shifted downward to 0.76 GHz from 1 GHz for n = 2. The reflection coefficient is -16.9 dB and the fractional bandwidth is 4.62%. The FSS array element dimensions in this case are 0.0152λ by 0.0152λ. While using five metallic layers (n = 5) and four dielectric layers, the resonant frequency is shifted to 0.6 GHz. The fractional bandwidth is 2.44%, and the reflection coefficient S_{11} is -9 dB. For this case, the size of the element is 0.012λ by 0.012λ.

Table II: Element size vs the number of metallic layers of single polarized FSSs

n	f (GHz)	BW	S21 (dB)	S_{11} (dB)	Thickness (mm)	Element size
2	1	6.23%	1.15	-19	0.147	0.02λ
3	0.76	4.62%	1.3	-16.9	0.284	0.0152λ
4	0.65	3.42%	1.9	-13	0.421	0.013λ
5	0.60	2.44%	2.6	-9.7	0.558	0.012λ

5 Dual polarized FSS

The FSS element proposed in last section is suitable for single polarized incident waves. The performance of the structure is different if the **E**-field of the incident wave is along the x-axis. To achieve dual-polarized performance, the proposed structure can be modified to the one shown in Fig. 11. This structure can be used for not only dual-polarization but also a greater fractional bandwidth. Here, the metallic structure on each layer is 90˚ rotationally symmetrical in the xy plane, so that the structure will achieve the same performance if the **E**-field of the incident wave is either in the x-axis or the y-axis direction. In the same way as before, the top and bottom layers are the same but flipped in the xy plane. Similarly, the dominant capacitor is the cross-layer C_{cc}, compared with the intrinsic capacitor. In this case only two pairs of patches will have a strong capacitance and the other two patches have relatively weak capacitance depending on the polarization.

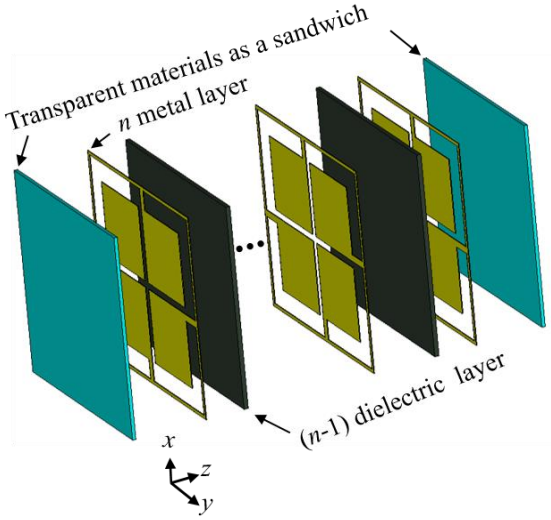

Fig. 11. Structure of the multi-layer bandpass FSS for dual polarisations.

The dimensions of the structure are: the gap *g* between adjacent patches is 0.2 mm; the width w of the short line connecting the patches is 0.2 mm and the loop is 0.1 mm. The periodic constant P of the array is 6 mm. The dimension of *b* is halved, which means the value of the capacitance is also about halved. The patch area is a^2 since $b = 2a$.

Table III: Element size vs number of metallic layers for the dual-polarized structure

n	*f* (GHz)	BW	S_{21} (dB)	S_{11} (dB)	Thickness (mm)	Element size
2	1.96	10.32%	0.56	-22.5	0.147	0.038λ
3	1.50	8.42%	1.23	-22.0	0.284	0.030λ
4	1.32	6.37%	1.62	-19.2	0.421	0.026λ
5	1.21	4.45%	1.86	-16.8	0.558	0.024λ

As mentioned, increasing the number of layers will shift the resonant frequency downward. The equivalent circuit of this structure is very similar to the single polarized one, taking into consideration that the value of the C_{cc} is halved. Table III shows the variation in the resonant frequency when increasing the number of layers, *n*. As can be seen from the table, the resonant frequency of the two-layer ($n = 2$) structure is 1.98 GHz. The same dielectric material of FR4 with 0.127 mm thickness is used in the design. The size of the array element is 0.0396λ × 0.0396λ. The resonant frequency of the structure with three metallic layers ($n = 3$) and two dielectric layers is 1.50 GHz. The array element size is 0.03λ × 0.03λ.

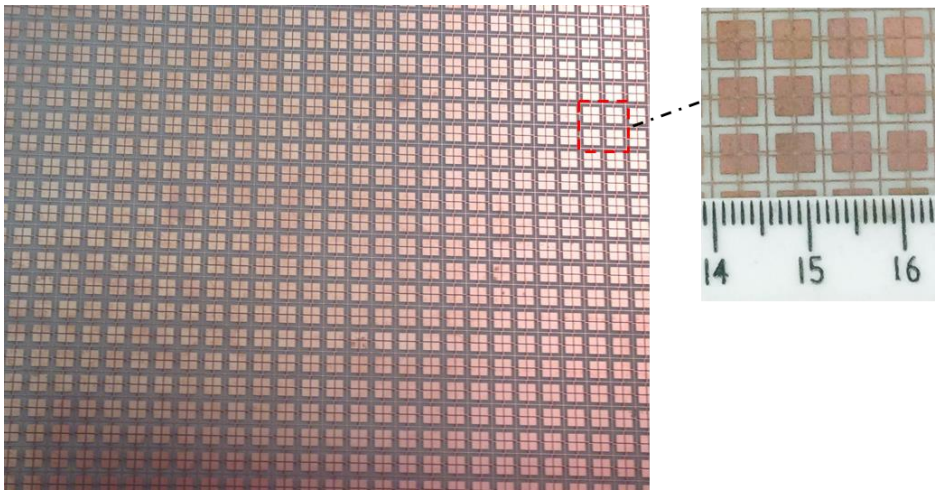

Fig. 12. Photograph of the prototype of the proposed FSS with $n = 2$.

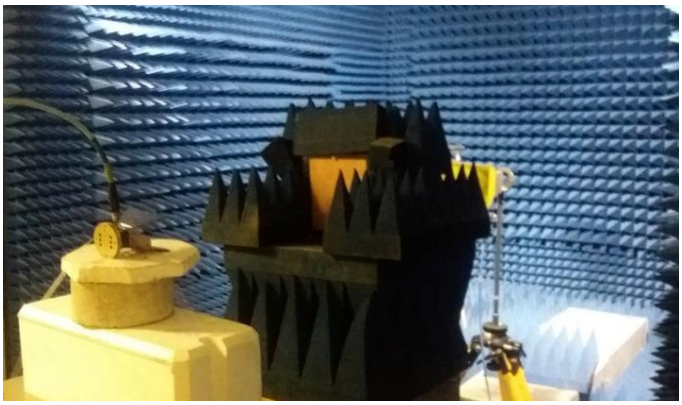

Fig. 13. Experimental setup to measure the transmission coefficient of the FSS.

6. Experimental results

A prototype of the proposed FSS as shown in Fig. 11 has been fabricated and measured to validate the design. The fabricated FSS is shown in Fig. 12. The size of the FSS prototype is 180 mm × 180 mm and it consists of 30 × 30 elements.

Two horn antennas and a vector network analyzer were used for the measurement. The measurement setup is shown in Fig. 13. The line of sight between the two antennas passes through the centre of the FSS prototype and the antennas are located about 70 cm away from the fixture to ensure the formation of uniform plane wave impinging upon the FSS structure. When carrying out the measurement at 60˚, the absorbers at the side were adjusted so as not to block the incident wave. Measurement of the fabricated FSS is performed in two steps. Firstly, the transmission response of the system without the FSS is measured. This measurement result is used to calibrate the FSS response. Secondly, the frequency response with the presence of the FSS structure is measured.

In the example of the FSS with two metallic layers (n = 2), the fabrication is performed by patterning the proposed shape on two sides of a 0.127 mm thick FR4 substrate. The measured performances with incident angles of 0^{o} and 60^{o} for this prototype are shown in Fig. 14. The measured insertion loss is 0.73 dB at the resonant frequency for normal incidence, which is mainly attributed to the dielectric and the metallic losses of the structure. The measured performance is compared with the simulated one. It can be seen that very good agreement has been achieved. The transmission with other incident angles up to 75^{o} was also measured. The measured performance is also in very good agreement with the simulated one. Such results are not shown in this figure to avoid having too many curves in the figure.

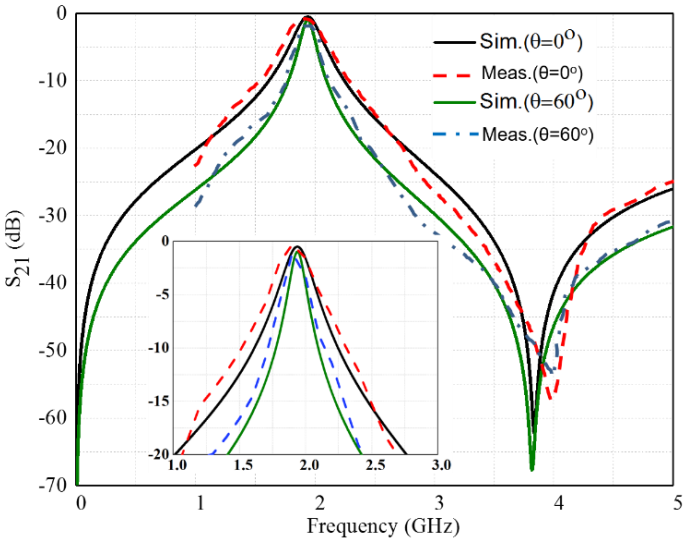

Fig. 14. Measured and simulated responses of the two-metallic-layer (n = 2) FSS under different incident angles.

7 Conclusions

An unconventional approach has been proposed to design miniaturized multi-layer FSSs. The overall thicknesses of the multi-layer FSSs presented are extremely small. As an example, the thickness of the FSS structure consisting of three metallic layers and two dielectric layers is less than 0.5 mm. Unlike traditional structures, the size of the proposed FSS element is smaller when the profile is lower.

The dimensions of the miniaturized element are much smaller than the wavelength at the resonant frequency, as small as 0.012λ × 0.012λ which is one of the smallest reported so far. For a two-metallic-layer structure, the size of the proposed dual polarized FSS element is 330 times smaller than the traditional patch-mesh structure.

The proposed approach to design miniaturized FSSs was experimentally verified by a prototype. The simulation and measurement results verify the stable frequency response of the proposed design. These advantages of the proposed structure can be useful for many applications where circuit compactness and having an extremely low profile are desired.

References

1 B. A. Munk, "Frequency selective surfaces theory and design. New York: Wiley-Interscience, 2000.
2 E. A. Parker, "The gentleman's guide to frequency selective surfaces." 17th QMW Antenna symposium pp. 1-18, 1991
3 F. Costa, A. Monorchio, and G. Manara, "Efficient analysis of frequency-selective surfaces by a simple equivalent-circuit model," IEEE Antennas and Propagation Magazine, vol. 54, no. 4, pp. 35-48, 2012
4 R. Ott, R. Kouyoumjian, and L. Peters, "Scattering by a two‐dimensional periodic array of narrow plate," Radio Science, vol. 2, no. 11, pp. 1347-1359, 1967.
5 B. Munk, and R. Luebbers, "Reflection properties of two-layer dipole arrays," IEEE Transactions on Antennas and Propagation, vol. 22, no. 6, pp. 766-773, 1974.
6 C. Winnewisser, F. Lewen, and H. Helm, "Transmission characteristics of dichroic filters measured by THz time-domain spectroscopy," Applied Physics a-Materials Science & Processing, vol. 66, no. 6, pp. 593-598, 1998.
7 S. Govindaswamy, J. East, F. Terry, E. Topsakal, J. L. Volakis, and G. I. Haddad, "Frequency-selective surface based bandpass filters in the near-infrared region," Microwave and Optical Technology Letters, vol. 41, no. 4, pp. 266-269, 2004
8 F. Bayatpur, and K. Sarabandi, "Single-layer high-order miniaturized-element frequency-selective surfaces," IEEE Transactions on Microwave Theory and Techniques, vol. 56, no. 4, pp. 774-781, 2008.
9 B. Schoenlinner, A. Abbaspour-Tamijani, L. C. Kempel, and G. M. Rebeiz, "Switchable low-loss RF MEMS Ka-band frequency-selective surface," IEEE Transactions on Microwave Theory and Techniques, vol. 52, no. 11, pp. 2474-2481, 2004.
10 D. Sievenpiper, L. J. Zhang, R. F. J. Broas, N. G. Alexopolous, and E. Yablonovitch, "High-impedance electromagnetic surfaces with a forbidden frequency band," IEEE Transactions on Microwave Theory and Techniques, vol. 47, no. 11, pp. 2059-2074, 1999.
11 K. Kumar, D. Sievenpiper, L. Zhang, R. Broas, N. Alexopolous, and E. Yablonovitch, "Comments on" High-impedance electromagnetic surfaces with a forbidden frequency band"[with reply]," IEEE Transactions on Microwave Theory and Techniques, vol. 49, no. 1, pp. 228, 2001.
12 T.-K. Wu, Frequency selective surface and grid array: Wiley-Interscience, 1995.
13 H. T. Liu, H. F. Cheng, Z. Y. Chu, and D. Y. Zhang, "Absorbing properties of frequency selective surface absorbers with cross-shaped resistive patches," Materials & Design, vol. 28, no. 7, pp. 2166-2171, 2007
14 T.-K. Wu, "Cassini frequency selective surface development," Journal of Electromagnetic Waves and Applications, vol. 8, no. 12, pp. 1547-1561, 1994.
15 Y. Rahmat-Samii, and A. N. Tulintseff, "Diffraction analysis of frequency selective reflector antennas," IEEE Transactions on Antennas and Propagation, vol. 41, no. 4, pp. 476-487, 1993.
16 Y. Rahmat-Samii, and M. Gatti, "Far-field patterns of spaceborne antennas from plane-polar near-field measurements," IEEE Transactions on Antennas and Propagation, vol. 33, no. 6, pp. 638-648, 1985.
17 G. Schennum, "Frequency-selective surfaces for multiple-frequency antennas," Microwave Journal, vol. 16, pp. 55-57, 1973.
18 https://www.slideshare.net/altairhtcus/cj-reddy-radomes-altairatc-final
19 S.-W. Lee, "Scattering by dielectric-loaded screen," IEEE Transactions on Antennas and Propagation, vol. 19, no. 5, pp. 656-665, 1971.
20 F. Sakran, Y. Neve-Oz, A. Ron, M. Golosovsky, D. Davidov, and A. Frenkel, "Absorbing frequency-selective-surface for the mm-wave range," IEEE Transactions on Antennas and Propagation, vol. 56, no. 8, pp. 2649-2655, 2008.
21 S. Chakravarty, R. Mittra, and N. R. Williams, "On the application of the microgenetic algorithm to the design of broad-band microwave absorbers comprising frequency-selective surfaces embedded in multilayered dielectric media," IEEE Transactions on Microwave Theory and Techniques, vol. 49, no. 6, pp. 1050-1059, 2001.
22 K. Sarabandi, and N. Behdad, "A frequency selective surface with miniaturized elements," IEEE Transactions on Antennas and Propagation, vol. 55, no. 5, pp. 1239-1245, 2007.
23 C. N. Chiu, and K. P. Chang, "A novel miniaturized-element frequency selective surface having a stable resonance," IEEE Antennas and Wireless Propagation Letters, vol. 8, pp. 1175-1177, 2009.
24 F. C. Huang, C. N. Chiu, T. L. Wu, and Y. P. Chiou, "A circular-ring miniaturized-element metasurface with many good features for frequency selective shielding applications," IEEE Transactions on Electromagnetic Compatibility, vol. 57, no. 3, pp. 365-374, 2015.
25 S. N. Azemi, K. Ghorbani, and W. S. T. Rowe, "Angularly stable frequency selective surface with miniaturized unit cell," IEEE Microwave and Wireless Components Letters, vol. 25, no. 7, pp. 454-456, 2015.
26 G. H. Yang, T. Zhang, W. L. Li, and Q. Wu, "A novel stable miniaturized frequency selective surface," IEEE Antennas and Wireless Propagation Letters, vol. 9, pp. 1018-1021, 2010.
27 W.-l. Li, G.-h. Yang, T. Zhang, and Q. Wu, "A novel frequency selective surface with ultra-wideband polarization selective response." Communication Technology (ICCT), 2010 12th IEEE International Conference on pp. 1315-1318.
28 M. B. Yan, S. B. Qu, J. F. Wang, J. Q. Zhang, A. X. Zhang, S. Xia, and W. J. Wang, "A novel miniaturized frequency selective surface with stable resonance," IEEE Antennas and Wireless Propagation Letters, vol. 13, pp. 639-641, 2014.
29 K. Sarabandi, and N. Behdad, "A frequency selective surface with miniaturized elements," IEEE Transactions on Antennas and Propagation, vol. 55, no. 5, pp. 1239-1245, 2007
30 C.-N. Chiu, and K.-P. Chang, "A novel miniaturized-element frequency selective surface having a stable resonance," IEEE Antennas and Wireless Propagation Letters, vol. 8, pp. 1175-1177, 2009
31 F. C. Huang, C. N. Chiu, T. L. Wu, and Y. P. Chiou, "A circular-ring miniaturized-element metasurface with many good features for frequency selective shielding applications," IEEE Transactions on Electromagnetic Compatibility, vol. 57, no. 3, pp. 365-374, Jun, 2015.
32 S. N. Azemi, K. Ghorbani, and W. S. T. Rowe, "Angularly stable frequency selective surface with miniaturized unit cell," IEEE Microwave and Wireless Components Letters, vol. 25, no. 7, pp. 454-456, 2015
33 G. H. Yang, T. Zhang, W. L. Li, and Q. Wu, "A novel stable miniaturized frequency selective surface," IEEE Antennas and Wireless Propagation Letters, vol. 9, pp. 1018-1021, 2010
34 M. Al-Joumayly, and N. Behdad, "A new technique for design of low-profile, second-order, bandpass frequency selective surfaces," IEEE transactions on antennas and propagation, vol. 57, no. 2, pp. 452-459, 2009.